

2024 S.T. Yau High School Science Award (Asia)

Research Report

The Team

Registration Number: Phy-135

Name of team member: WANG Yunze

School: Raffles Institution

Country: Singapore

Name of supervising teacher: SZE Guan Kheng

Job Title: Lecturer

School: Raffles Institution

Country: Singapore

Modal Frequencies in a nonlinear beam-magnet coupled oscillator system

Date

28 July 2024

2024 S.-T. Yau High School Science Award
仅用于2024丘成桐中学科学奖公示

Modal Frequencies in a nonlinear beam-magnet coupled oscillator system

Wang Yunze

Abstract

The motion of a nonlinear coupled oscillator system consisting of two leaf springs secured to a non-magnetic base with magnets attached to the upper ends such they repel and are free to move was investigated. My results showed that the system exhibits the beats phenomenon, and the frequency shows a dependence on initial conditions. I hence hypothesized this sensitivity on initial conditions is due to two sources of nonlinearities: geometric nonlinearity during large deflections of the leaf springs and the nonlinearity in the magnetic force. To test this hypothesis, a nonlinear mathematical model was developed, accounting for nonlinear beam effects up to third order and fully solving the nonlinear magnetic force using a current cylinder model, accounting for the tilting of the magnets. An approximate linear model was also developed for comparison. The theoretical models were validated experimentally by investigating the dynamic motion of the springs through time, as well as how the modal frequencies in the system depend on the initial displacement, the length of the spring, and the distance between the springs. The more accurate nonlinear model I derived shows good agreement with experimental results while the linear theory does not, highlighting the importance of nonlinearities in this system. An improved understanding of these nonlinear systems could lead to advancements in design and efficiency, and safety in various applications such as energy harvesting.

Keywords: coupled oscillator, nonlinear vibrations, geometric nonlinearity, magnetically coupled dual beams, large deformation of cantilever beam

Acknowledgement

I would like to thank the International Young Physicist Tournament (IYPT) for proposing the magnetic mechanical oscillator as a competition problem, which inspired the work of this project, much of which was presented at Online Young Physicist Tournament (OYPT) 2023 by the Singapore team. I greatly appreciate the insightful discussions with the OYPT 2023 Singapore team members and coaches, as well as Mr. Sze Guan Kheng from Raffles Institution, and Dr. Koh Teck Seng from Nanyang Technological University.

Commitments on Academic Honesty and Integrity

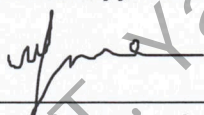
We hereby declare that we

1. are fully committed to the principle of honesty, integrity and fair play throughout the competition.
2. actually perform the research work ourselves and thus truly understand the content of the work.
3. observe the common standard of academic integrity adopted by most journals and degree theses.
4. have declared all the assistance and contribution we have received from any personnel, agency, institution, etc. for the research work.
5. undertake to avoid getting in touch with assessment panel members in a way that may lead to direct or indirect conflict of interest.
6. undertake to avoid any interaction with assessment panel members that would undermine the neutrality of the panel member and fairness of the assessment process.
7. observe the safety regulations of the laboratory(ies) where the we conduct the experiment(s), if applicable.
8. observe all rules and regulations of the competition.
9. agree that the decision of YHSA(Asia) is final in all matters related to the competition.

We declare that this project has been used in the past to participate in the Singapore Science and Engineering Fair (SSEF) in March 2024.

We understand and agree that failure to honour the above commitments may lead to disqualification from the competition and/or removal of reward, if applicable; that any unethical deeds, if found, will be disclosed to the school principal of team member(s) and relevant parties if deemed necessary; and that the decision of YHSA(Asia) is final and no appeal will be accepted.

(Signatures of full team below)



Name of team member: WANG Yunze



Name of supervising teacher: Mr SZE Guan Kheng

Noted and endorsed by

(signature) 



AARON LOH
Principal
Raffles Institution

Name of school principal: Mr Aaron LOH

Modal frequencies in a nonlinear beam-magnet coupled oscillator system

Wang Yunze

(Dated: 28 July 2024)

The motion of a nonlinear coupled oscillator system consisting of two leaf springs secured to a non-magnetic base with magnets attached to the upper ends such they repel and are free to move was investigated. My results showed that the system exhibits the beats phenomenon, and the frequency shows a dependence on initial conditions. I hence hypothesized this sensitivity on initial conditions is due to two sources of nonlinearities: geometric nonlinearity during large deflections of the leaf springs and the nonlinearity in the magnetic force. To test this hypothesis, a nonlinear mathematical model was developed, accounting for nonlinear beam effects up to third order and fully solving the nonlinear magnetic force using a current cylinder model, accounting for the tilting of the magnets. An approximate linear model was also developed for comparison. The theoretical models were validated experimentally by investigating the dynamic motion of the springs through time, as well as how the modal frequencies in the system depend on the initial displacement, the length of the spring, and the distance between the springs. The more accurate nonlinear model I derived shows good agreement with experimental results while the linear theory does not, highlighting the importance of nonlinearities in this system. An improved understanding of these nonlinear systems could lead to advancements in design and efficiency, and safety in various applications such as energy harvesting.

I. INTRODUCTION

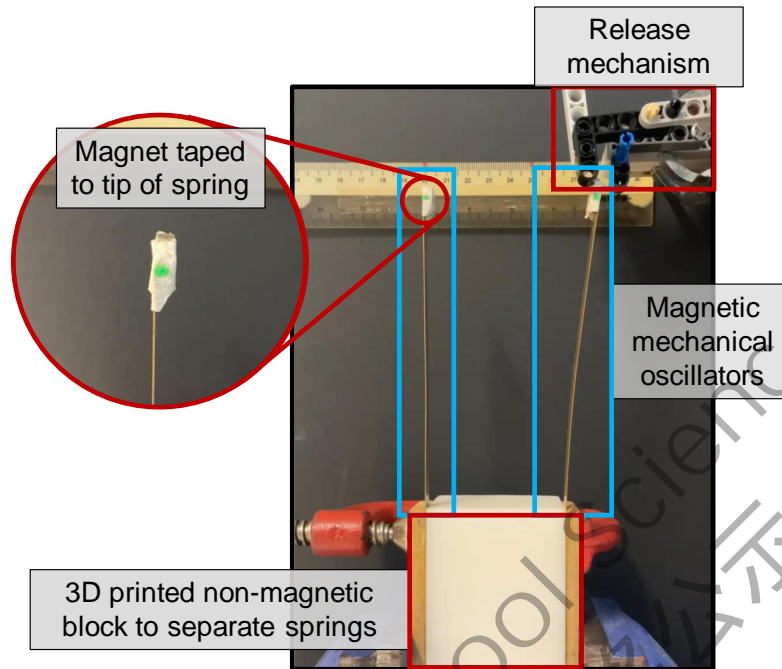


FIG. 1. The magnetic mechanical oscillator (MMO) setup. The setup consists of two cantilever beams clamped to a non-magnetic base, then attaching magnets to the upper ends such that they repel and are free to move. A lever release mechanism is used to minimize the initial velocity given during release.

A coupled oscillator system is one where two or more oscillators are coupled together via another force, such that the oscillations of one oscillator will affect the oscillation of the others. In this paper, I will be focusing on the case of two oscillators. A *linear* coupled oscillator system is one where the restoring force on the oscillators and the coupling force is a linear function of the displacements. Linear coupled oscillator systems are well established, with the resulting motion being the superposition of two harmonic oscillations whose frequencies are known as the *modal frequencies*, leading to interesting motion such as beats¹.

However, these results no longer apply when the system is nonlinear². Compared to the linear case, it is possible to obtain more complex motion where the modal frequencies are not constants of the system but rather functions of the amplitude of oscillations.

In this paper, I investigated a nonlinear coupled oscillator system which I named the Magnetic Mechanical Oscillator (MMO), comprising two cantilever beams clamped to a

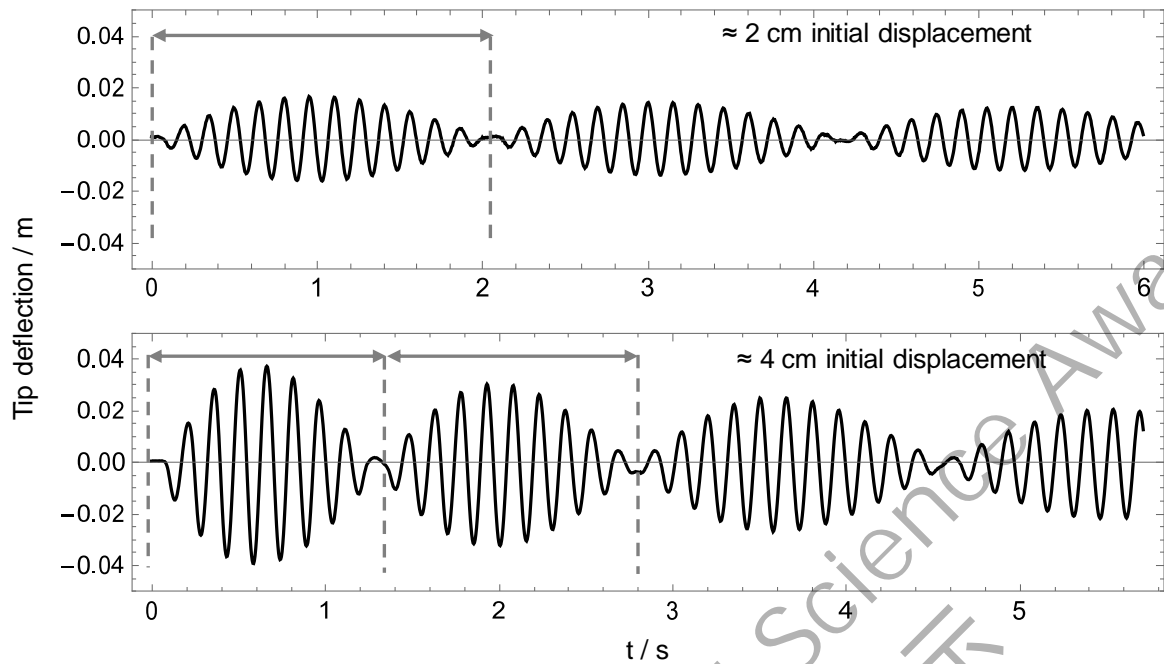


FIG. 2. Horizontal deflection of tip of the springs against time for two identical setups released with a ≈ 2 cm initial displacement (top) and ≈ 4 cm initial displacement (bottom). The dashed vertical lines represent a “beat”. The frequency depends not just on the system parameters but also initial conditions. As the amplitude of oscillations decreases due to damping, the beat frequency decreases as well. The average frequency decreases too, although this is not as obvious from the plot.

non-magnetic base with magnets attached to the upper ends of the beams of such that they repel and are free to move (Fig. 1)³. The two cantilever beams act as oscillators that are coupled together via the magnetic force between the magnets at the tip.

This MMO system exhibited the beats behavior where there was a “fast” oscillation at a high frequency which I called the *average frequency*, whose amplitude was modulated by a “slow” oscillation at the *beat frequency* (Fig. 2 top).

There are two sources of nonlinearities in the MMO system, one due to the nonlinear force between the two magnets, and the other due to geometric nonlinearities in the cantilever beams at larger deflections. These nonlinearities cause the beat frequency to be amplitude-dependent, which is not the case for linear coupled oscillators (Fig. 2 bottom).

The whole concept of normal modes is based off the linearity of the system. If the system is nonlinear, the superposition principle no longer applies and the solution is not

just the sum of the normal mode oscillations.

However, one possible way to define a *nonlinear normal mode* is as synchronous periodic solutions of the nonlinear equations of motion, where all coordinates of the system oscillate with the same period, reaching the maximum and minimum at the same time⁴.

If the system is linearizable with weak nonlinearities, these nonlinear model modes approach the classical normal modes of the linearized system as the nonlinearities tend to zero⁴. These normal modes are the ones that we investigate in this paper.

I developed two mathematical models for the MMO system. First, I approximated it to the linear coupled oscillator system by linearizing simplified equations of motion, then more accurately model the system using a large deflection Euler-Bernoulli beam model and modelling the magnets as current cylinders, accounting for nonlinearities in both the beam and the magnet. I then experimentally verified both models, showing that the linearized model is inaccurate and cannot fully describe the motion, highlighting nonlinearities in the system.

II. MATHEMATICAL MODELING OF MMO SYSTEM

A. Linear approximation

1. *Linear leaf springs*

The leaf spring can be approximated as an ideal linear spring. Throughout this paper, a prime x' will be used to represent a spatial derivative dx/ds and an overdot \dot{x} will be used to represent a temporal derivative dx/dt .

Consider a vertical cantilevered beam of length L , Young's modulus E , second moment of area I , and mass per unit length μ with a tip mass m attached. $v(s, t)$ is the horizontal displacement of the beam at distance s along the beam.

The dynamic equation of motion for such a beam can be written as

$$EIv'''' + \mu\ddot{v} = 0 \tag{1}$$

where the boundary conditions are

$$v(0, t) = 0, \quad (2)$$

$$v'(0, t) = 0, \quad (3)$$

$$v''(L, t) = 0, \quad (4)$$

$$EIv'''(L, t) = m\ddot{v}(L, t). \quad (5)$$

Equations (2) and (3) represents the fixed end at $s = 0$, while Eq. (4) represents the free end at $s = L$. The tip mass is included in Eq. (5).

Irvine⁵ showed that this system is approximately equivalent to a ideal spring-mass system with effective spring constant

$$k_s = \frac{3EI}{L^3} \quad (6)$$

and effective mass

$$m_{\text{eff}} = 0.2246\mu L + m. \quad (7)$$

2. Linear magnetic force

Consider two cylindrical magnets with radius R , height H and magnetizations M_1 and M_2 respectively. We can approximate them as magnetic dipoles with a dipole moment $(\pi R^2 H)M_\alpha$ ($\alpha = 1, 2$).

Assuming the two magnets remain coaxial even when the cantilever beams bend, the force between the dipoles is

$$F_{\text{mag}}(d) = \frac{3\mu_0 M_1 M_2 (\pi R^2 H)^2}{2\pi d^4}. \quad (8)$$

Defining the distance between the cantilever beams (which is approximately distance between the two magnets at equilibrium) as d_0 , we can do a Taylor expansion to 1st order around d_0 to obtain a linear approximation of the magnetic force which resembles the linear spring equation:

$$F_{\text{mag}}(d) = -k_m d + c_m + \mathcal{O}(d^2) \quad (9)$$

where

$$k_m = \frac{6\mu_0 M_1 M_2 \pi H^2 R^4}{d_0^5}, \quad c_m = \frac{15\mu_0 M_1 M_2 \pi H^2 R^4}{2d_0^4}. \quad (10)$$

3. *Linearised equations of motion*

Hence, we can write down the linearized equations as such:

$$m_{\text{eff}}\ddot{v}_1 = -k_s v_1 + k_m(v_2 - v_1 + d_0) - c_m, \quad (11)$$

$$m_{\text{eff}}\ddot{v}_2 = -k_s v_2 - k_m(v_2 - v_1 + d_0) + c_m. \quad (12)$$

This is similar to the traditional coupled oscillator with the addition of a constant term in the force exerted by the “middle spring”, since the magnetic repulsion force is never zero.

If we apply the initial conditions of $v_1(0) = 0$, $v_2(0) = a$, and $\dot{v}_1(0) = \dot{v}_2(0) = 0$ this set of equations has the solution

$$v_1 = +A_0 + A_1 \cos \omega_1 t + A_2 \cos \omega_2 t, \quad (13)$$

$$v_2 = -A_0 + A_1 \cos \omega_1 t - A_2 \cos \omega_2 t, \quad (14)$$

$$(15)$$

where

$$A_0 = \frac{k_m d_0 - c_m}{2k_m + k_s}, \quad (16)$$

$$A_1 = \frac{a}{2}, \quad (17)$$

$$A_2 = \frac{2c_m - 2(a + d_0)k_m - ak_s}{2(2k_m + k_s)}, \quad (18)$$

and the two modal frequencies are:

$$\omega_1 = \sqrt{\frac{k_s}{m_{\text{eff}}}}, \quad (19)$$

$$\omega_2 = \sqrt{\frac{k_s + 2k_m}{m_{\text{eff}}}}. \quad (20)$$

The solution is the superposition of two cosines, with the addition of a constant offset term. This is not surprising since the equations of motion are still linear.

4. *Beats*

For beams of length $L = 12$ cm, separation distance $d_0 = 4.5$ cm, release amplitude $a = 1$ cm and the other constants described in Sec. III A, the values of “spring constants” are $k_s = 4.15$ N/m, $k_m = 0.702$ N/m and $c_m = 0.0790$ N, so the values for the amplitudes

can be calculated as $A_0 = 8.53 \times 10^{-3}$ m, $A_1 = 5 \times 10^{-3}$ m, and $A_2 = 3.53 \times 10^{-3}$ m. Using the approximation $A_1 \approx A_2$, Eqs. (13) and (14) become

$$v_1 = +A_0 + A_1 \cos \omega_1 t + A_1 \cos \omega_2 t, \quad (21)$$

$$v_2 = -A_0 + A_1 \cos \omega_1 t - A_1 \cos \omega_2 t. \quad (22)$$

It is well known that we can rewrite Eqs. (21) and (22) using the sum-to-product trigonometric identity $\cos \theta + \cos \varphi = 2 \cos ((\theta + \varphi)/2) \cos ((\theta - \varphi)/2)$ to become

$$v_1(t) = +A_0 + 2A_1 \cos(\omega_{\text{avg}} t) \cos\left(\frac{\omega_{\text{beat}}}{2} t\right), \quad (23)$$

$$v_2(t) = -A_0 - 2A_1 \sin(\omega_{\text{avg}} t) \sin\left(\frac{\omega_{\text{beat}}}{2} t\right), \quad (24)$$

where

$$\omega_{\text{avg}} \equiv \frac{\omega_1 + \omega_2}{2}, \quad (25)$$

$$\omega_{\text{beat}} \equiv |\omega_1 - \omega_2|. \quad (26)$$

When the two modal frequencies ω_1 and ω_2 are similar, the difference between them is small and the beat frequency ω_{beat} is small, leading to the beating phenomenon. Eqs. (25) and (26) are the mathematical expressions for the beat and average frequency defined in the introduction. The factor of half in the definition for ω_{beat} is omitted because the peaks in the amplitude appears twice every period, so we have defined the beat frequency is double the frequency of the cosine.

5. Limitations

Note that this linear theory fails to account for more than just the nonlinearities that arise from finite amplitudes. It assumes the magnets remain coaxial to each other, although in reality the magnets become tilted when the springs bend, causing a decrease in the magnetic force. The effects of gravity on the beam were also neglected. Since the beams are vertically clamped at the bottom, gravity will oppose the restoring force of the beam and cause a slight decrease in the frequency of oscillations, which is demonstrated in Appendix D.

B. Full nonlinear model

Now, I will move on to the full nonlinear model of the MMO system, taking into account both nonlinearities in the large deflections of the cantilevered beam as well as

the magnetic force.

1. Large deflection beam model

The equations of motion for a vertical cantilever beam (see Appendix A for the derivation) are:

$$\begin{aligned} \mu \ddot{v} = & -c_D \dot{v} - EI (v'''' + [v'(v'v'')]') - mgv'' - \frac{\mu}{2} \frac{\partial}{\partial s} \left(v' \int_L^s \int_0^\theta \frac{\partial^2}{\partial t^2} (v'^2) dy d\theta \right) \\ & + \mu g(v' + (s-L)v'') + \frac{mv''}{2} \int_0^L \frac{\partial^2}{\partial t^2} (v'^2) ds \mp (\mathbf{F}_{\text{mag}} \cdot \hat{\mathbf{e}}_y) v'', \end{aligned} \quad (27)$$

$$\begin{aligned} m\ddot{v}|_{s=L} = & mgv' - \frac{mv''}{2} \int_0^L \frac{\partial^2}{\partial t^2} (v'^2) dy + EI (v'''' + v''''v'^2 + v''^2v') \\ & \pm (\mathbf{F}_{\text{mag}} \cdot \hat{\mathbf{e}}_x) \pm (\mathbf{F}_{\text{mag}} \cdot \hat{\mathbf{e}}_y) \left(v' + \frac{1}{2}v'^3 \right) \Big|_{s=L}, \end{aligned} \quad (28)$$

$$v''(L, t) = 0, \quad (29)$$

$$v(0, t) = v'(0, t) = 0. \quad (30)$$

where s , v , u , ψ are defined in Fig. 3 and y and θ are dummy integration variables. Equation (27) is the equation of motion for the beam, taking into account nonlinearities up to third order. Equations (28)–(30) are the boundary conditions.

2. Current cylinder magnet model

The magnetic dipole approximation becomes inaccurate as the magnets used were cylindrical with finite size. We can more accurately model the magnets as current cylinders with surface current K equal in magnitude to the magnetization, assuming the magnetization is uniform in the axial direction⁶.

a. Coordinate transforms There are three degrees of freedom for the magnets: the horizontal and vertical displacements, as well as the tilt angle between the two magnets. I denoted the frame of the left magnet the unprimed coordinates (x, y, z) and the frame of the right magnet the primed coordinates (x', y', z') , where $\mathbf{r}_0 = (x_0, 0, z_0)$ is the vector pointing from the origin of the unprimed to the origin of the primed coordinate system (Fig. 4). The centers of the magnets always lie in the plane with $y = 0$ since the beams

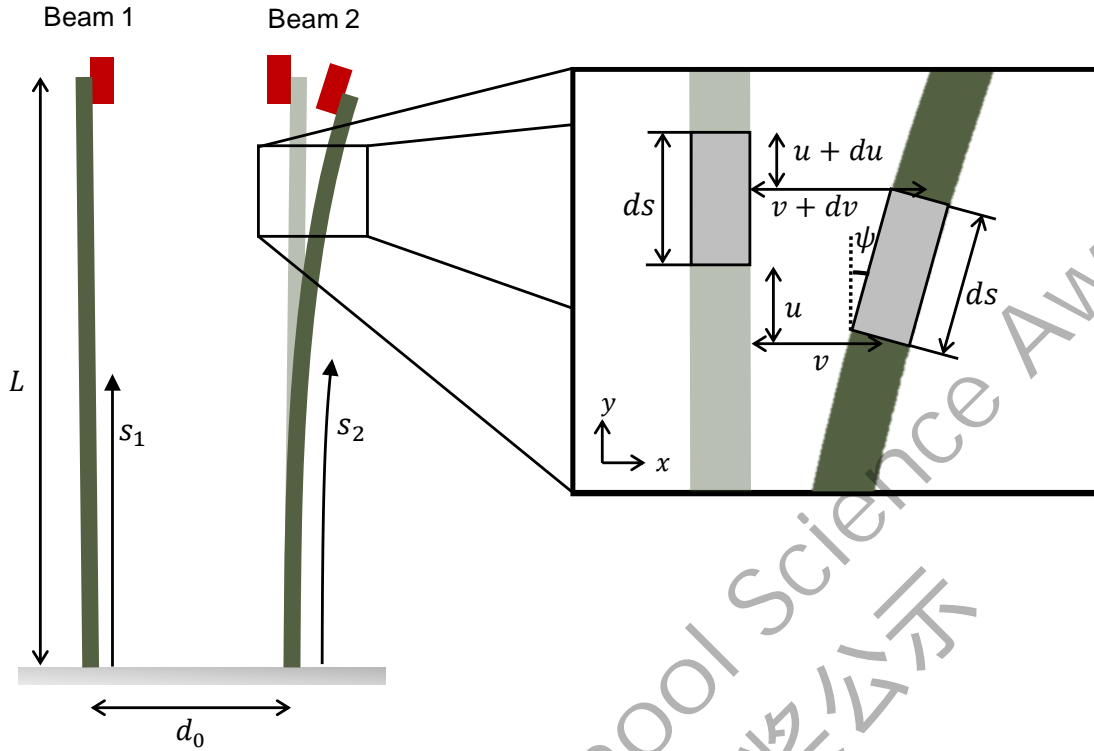


FIG. 3. s_1 and s_2 are the coordinates along the two beams. Since the two beams are identical, I will drop the subscripts and focus only one beam. A global coordinate system is defined where x points to the right, y is up and z is out of the page. $v(s, t)$ is the horizontal displacement of a beam element, $u(s, t)$ is the vertical displacement, and $\psi(s, t)$ is the angle the beam makes with the vertical.

can only oscillate in that plane. The two frames are related by the coordinate transform

$$\begin{bmatrix} x' \\ y' \\ z' \end{bmatrix} = \begin{bmatrix} \cos \theta & 0 & -\sin \theta \\ 0 & 1 & 0 \\ \sin \theta & 0 & \cos \theta \end{bmatrix} \begin{bmatrix} x \\ y \\ z \end{bmatrix} \quad (31)$$

Note that the (x, y, z) here are unrelated to the global coordinate system (x, y, z) used in the beam formulation. The values of x_0 and z_0 are related to the beam variables by

$$\begin{bmatrix} x' \\ z' \end{bmatrix} = \begin{bmatrix} \sin \psi_1 & \cos \psi_1 \\ -\cos \psi_1 & \sin \psi_1 \end{bmatrix} \begin{bmatrix} u_2 - u_1 \\ v_2 - v_1 + d_0 - H \end{bmatrix} \quad (32)$$

where the subscripts 1 and 2 denote the left and right beams respectively, and the values of u and v are evaluated at the tip of the beams, and θ is simply

$$\theta = \psi_2 - \psi_1. \quad (33)$$

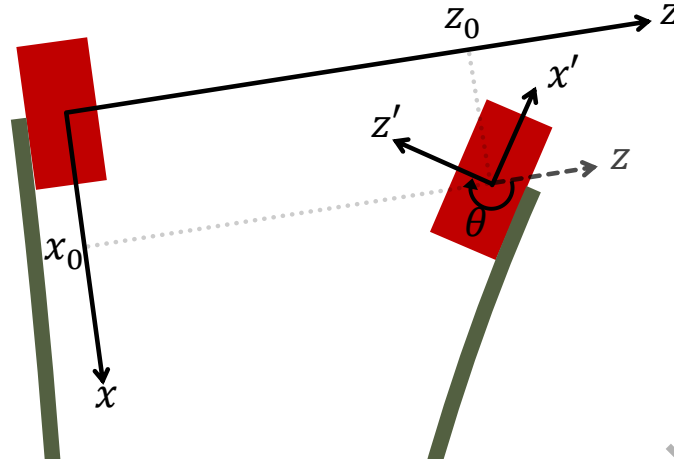


FIG. 4. The definitions of the unprimed and primed frames used in the magnetic force computation. The origin of the primed frame is at a coordinate $(x_0, 0, z_0)$ in the unprimed frame. The centers of the magnets will always lie in the plane $y = 0$ since the beams can only oscillate in that plane.

b. Magnetic field According to Derby and Olbert⁶, the radial and axial magnetic field produced by such a current cylinder with thickness $2b$ and radius a is

$$B_r = B_0[\alpha_+ C(k_+, 1, 1, -1) - \alpha_- C(k_-, 1, 1, -1)] \quad (34)$$

and

$$B_z = \frac{B_0 a}{a + r} [\beta_+ C(k_+, \gamma^2, 1, \gamma) - \beta_- C(k_-, \gamma^2, 1, \gamma)] \quad (35)$$

respectively, where

$$B_0 = \frac{\mu_0 n I}{\pi}, \quad (36)$$

$$z_{\pm} = z \pm b, \quad (37)$$

$$\alpha_{\pm} = \frac{a}{\sqrt{z_{\pm}^2 + (\rho + a)^2}}, \quad (38)$$

$$\beta_{\pm} = \frac{z_{\pm}}{\sqrt{z_{\pm}^2 + (\rho + a)^2}}, \quad (39)$$

$$\gamma = \frac{a - \rho}{a + \rho}, \quad (40)$$

$$k_{\pm} = \sqrt{\frac{z_{\pm}^2 + (a - \rho)^2}{z_{\pm}^2 + (a + \rho)^2}}. \quad (41)$$

These expressions give the magnetic field produced by the left magnet (in the unprimed frame) in cylindrical coordinates.

c. *Magnetic force* To determine the magnetic force, the Lorentz force

$$\mathbf{F}_{\text{mag}} = \iint_S \mathbf{K} \, dS \times \mathbf{B} \quad (42)$$

can then be integrated over the surface S of the other magnet to find the magnetic force. Here, \mathbf{B} is the magnetic field produced by the left magnet, and $\mathbf{K} = \mathbf{M} \times \hat{\mathbf{n}}$ is the surface current of the right magnet with a magnetization of M . For ease of integration, we do this in integral in the primed frame in cylindrical coordinates:

$$\mathbf{F}_{\text{mag}} = R \int_{-H/2}^{H/2} \int_0^{2\pi} (\mathbf{M} \times \hat{\boldsymbol{\varphi}}) \times \mathbf{B} \, d\varphi \, dz'. \quad (43)$$

By computing this numerically using the coordinate transforms, I account for the fact that the magnets are tilted and vertically displaced from each other when the beams bend, hence addressing this limitation in the simplified linear model.

3. Numerical solution

The 4th-order nonlinear partial differential equation for the beams and the integrals for the magnetic force and are solved numerically.

At each time step, the magnetic force is computed using Eq. (42). Then, Eqs. (27) – (30) are solved for each beam, by discretizing each beam into 15 evenly spaced grid points and using a 4th-order finite-difference (central-difference) scheme⁷ to obtain the spatial derivatives. A backwards Euler method⁸ is used in the time domain with a small time step of $\Delta t = 2 \times 10^{-5}$ s to minimize numerical error.

III. EXPERIMENTAL VERIFICATION AND DISCUSSION

A. Experimental setup

I experimentally constructed the MMO system by clamping two brass plates with a measured flexural rigidity of $EI = 2.39 \times 10^{-3} \text{ N m}^2$ (refer to Appendix B for how this value was measured) and mass per unit length $\mu = 0.0248 \text{ kg m}^{-1}$ to a 3D printed block to accurately control the distance between the two springs (Fig. 1). The springs were aligned using a flat surface when clamping. The right spring was then released using a lever to ensure minimal initial release velocity to set the system into oscillations. A high-speed camera recorded the phenomenon at 250 FPS and the positions of the magnets were tracked by a small green dot on the magnets using image processing techniques.

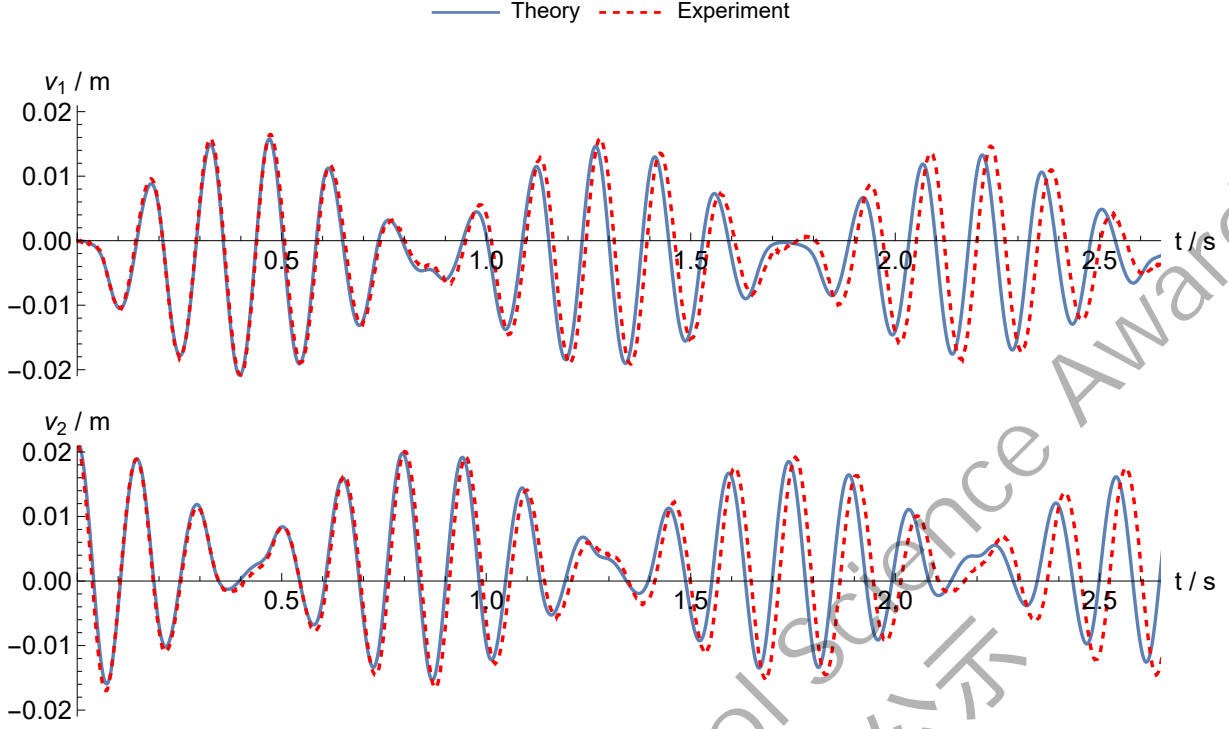


FIG. 5. Horizontal deflection of the tip of the left and right springs (top and bottom plot respectively) with parameter values described in Sec. III A and a length of $L = 12$ cm and separation distance $d_0 = 4.5$ cm, released with an initial amplitude of $A = 2$ cm. Error bars are omitted for visualization purposes.

In these experiments, cylindrical magnets were used with a mass of $m = 1.774$ g, radius $R = 0.5$ cm, height $H = 0.3$ cm, and the magnetization of the magnets were characterized to be $M_1 = 0.944 \times 10^6$ A m $^{-1}$ and $M_2 = 1.03 \times 10^6$ A m $^{-1}$ respectively by measuring the axial magnetic field strength using a hall probe and fitting it to Eq. 35.

B. Dynamic trajectory

For a beam length of $L = 12$ cm and separation distance of $d_0 = 4.5$ cm, the two modal frequencies in Eqs. (19) and (20) are $\omega_1 = \sqrt{k_s/m_{\text{eff}}} = 41.2$ rad s $^{-1}$ and $\omega_2 = \sqrt{(k_s + 2k_m)/m_{\text{eff}}} = 47.7$ rad s $^{-1}$.

Since the two modal frequencies are similar to each other, as explained in Sec. II A 4, we observe the beats phenomenon with a beat frequency $\omega_{\text{beat}} = \omega_2 - \omega_1 = 6.47$ rad s $^{-1} = 1.03$ Hz.

In the plot of horizontal deflection v of the tip against time (Fig. 5), we observe the beats phenomenon. The increasing deviations between the theory and experiment as time

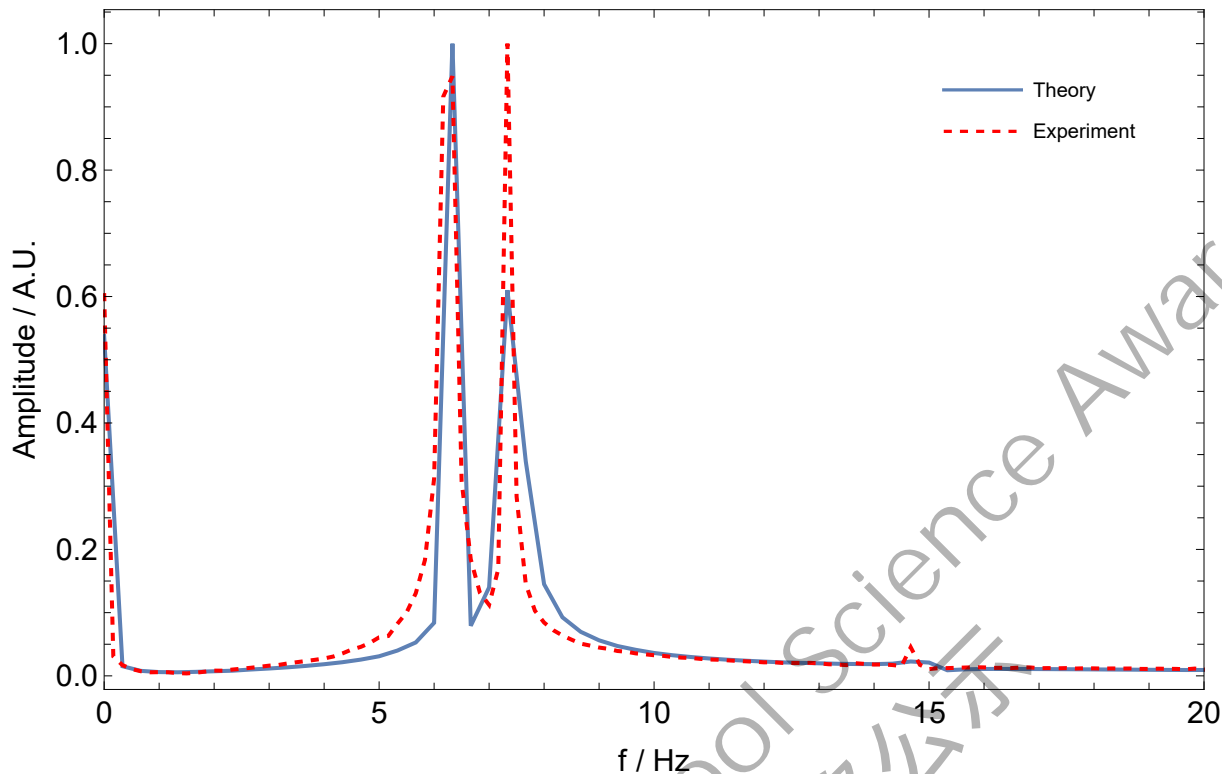


FIG. 6. The discrete Fourier transform of the graph of tip deflection against time, with the peak amplitude normalized to be 1. It displays two main peaks representing the system's two modal frequencies. Additionally, a minor peak near 15 Hz indicates the weak nonlinearities in the system, while the peak at 0 represents the equilibrium position being slightly deflected from the springs being perfectly vertical due to the magnetic force.

goes on are likely due to small errors in the measurement of the value of flexural rigidity EI or magnetization M which led to the predicted modal frequencies to be slightly higher than the actual value.

Taking the discrete Fourier transform of the deflection-time plot (Fig. 6), we observe two main peaks, corresponding to the two modal frequencies respectively. The small peak at around 15 Hz is due to the weak nonlinearities in the system causing the oscillations to not be exactly harmonic (i.e. sinusoidal). There is also a peak at 0, which represents the fact that the beams are not oscillating about the point where they are vertical, but rather the equilibrium position is slightly offset due to the always-present magnetic repulsion force. This corresponds to the first constant term in Eqs. (21) and (22).

We see the nonlinear theory presented is able to accurately predict the modal frequencies present.

C. Varying amplitude

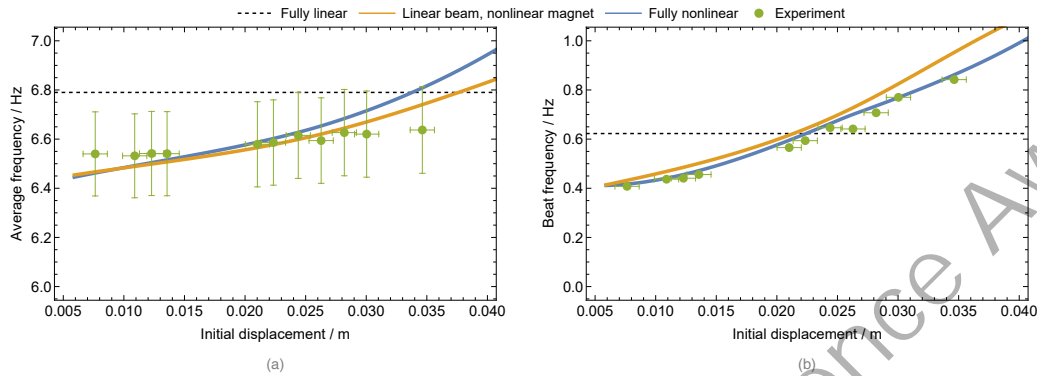


FIG. 7. The dependence of the (a) average and (b) beat frequency on the initial displacement at release, showcasing the frequency's dependence on the amplitude of oscillations. A length of $L = 12$ cm and separation distance of $d_0 = 5.5$ cm was used. The yellow line is computed with the nonlinear terms in the beam removed, leaving just the nonlinearity in the magnet. The blue line includes all nonlinear terms. The fully linear theory (dashed line) is included for comparison. The method for obtaining the beat and average frequency is described in Appendix C.

A key idea from II A 4 is that the modal frequencies are dependent solely on the parameters of the system (i.e. the spring constants and masses). However, this is not true in general for the nonlinear case. Recall from Fig. 2 that damping causes the amplitude to decrease, which causes the beat and average frequencies to decrease as well (Fig. 7).

In Fig. 7, I have plotted the prediction from the fully linear theory, as well as the theory with the nonlinear terms in the beam equations (Eqs. 27 – 30) removed, but keeping the full nonlinear theory from the magnets. Comparing that to the fully nonlinear line, it is apparent that the nonlinearities in the beam are significant in this setup. For a comparison of the orders of magnitude of terms, see Appendix E.

As expected, the linear theory prediction remains constant.

The reason why the beat and average frequencies increase as the amplitude increases is the magnets move closer to each other, so the magnetic coupling force becomes much stronger due to the nonlinear nature of the magnetic force, hence the second modal frequency ω_2 increases and both the average and beat frequency increases.

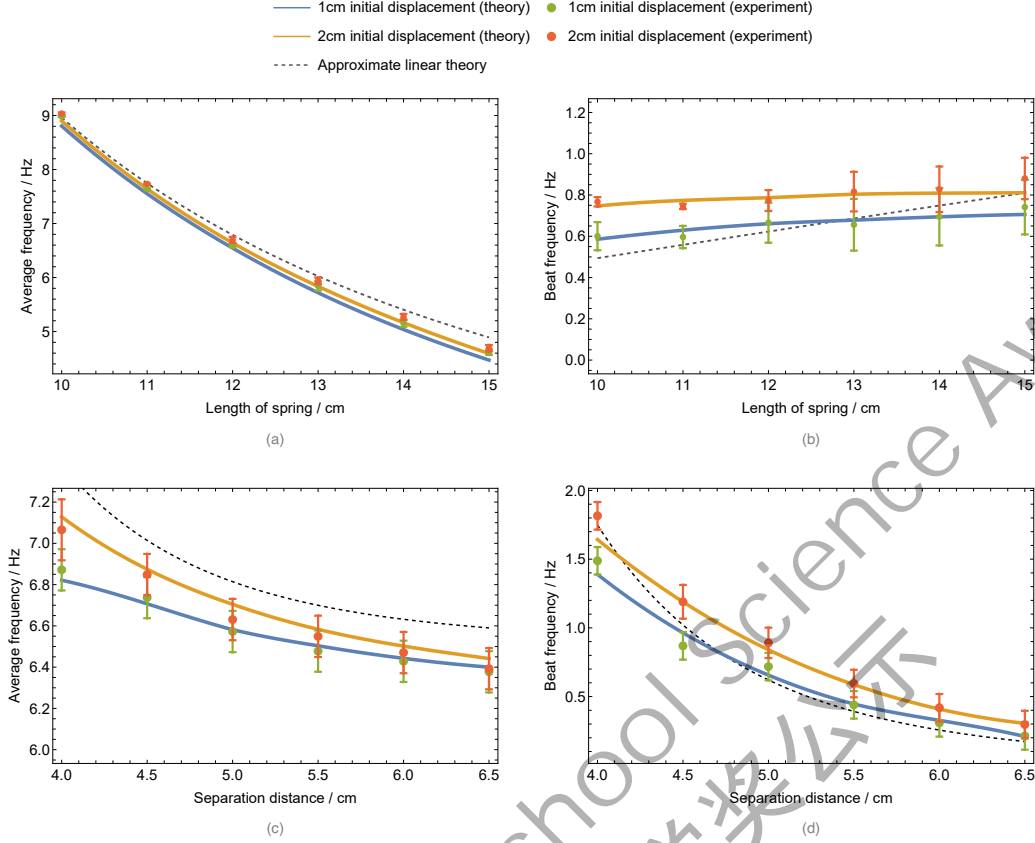


FIG. 8. The average and beat frequencies and their dependence on: (a), (b) the length of the beams L , and (c), (d) the separation distance between the beams d_0 . Two sets of data were taken with initial displacements of 1 cm and 2 cm to highlight the frequencies' dependence on initial conditions. The theory lines are computed using the full nonlinear theory including both magnet and beam nonlinearities. The fully linear approximation is shown in dashed line for comparison, which does not predict an amplitude dependence. All theory lines were computed with the values described in Sec. III A.

D. Varying beam length

Increasing the length of the beams causes the average frequency to decrease and the beat frequency to increase (Figs. 8a and 8b). This can be qualitatively explained by using the linear approximation of the system (Sec. II A). When the length of the beam increases, the effective beam constant of the leaf beam k_s decreases (Eq. 6). Intuitively, a longer beam is easier to bend than a shorter one.

When k_s increases, both modal frequencies ω_1 and ω_2 increase (Eqs. 19 and 20). However, since $\omega_1 < \omega_2$, ω_1 will increase more than ω_2 . As such, the difference between them actually decreases and hence the beat frequency $\omega_{\text{beat}} = \omega_2 - \omega_1$ decreases.

E. Varying separation distance

Increasing the separation distance d_0 between the two beams causes both the average and beat frequency to decrease (Figs. 8c and 8d). The beat frequency decreases because the coupling strength between the two oscillators is weaker when the distance is farther, so the kinetic energy takes a longer time to be completely transferred from one to the other.

When the separation distance increases, the effective spring constant for the magnet k_m (Eq. 10) increases. In that case, ω_1 stays constant while ω_2 increases, so both the average and the difference between the two modal frequencies increases and the average and beat frequency increases.

IV. CONCLUSION

In this paper, I have investigated how the modal frequencies are affected by different parameters in a nonlinear continuum system, showing that the beat and average frequencies increase as the amplitude of the system increases, which is characteristic of nonlinear systems.

This work highlights the importance of nonlinearities in coupled oscillator systems. Contrary to linear systems, these nonlinear systems are rarely discussed in most undergraduate textbooks because the nonlinear equations of motion rarely have analytical solutions⁹. However, it is of important educational value to show the additional insights that nonlinearities that occur in real world systems. An improved understanding of these nonlinear systems could lead to advancements in design, efficiency, and safety of various mechanical structures.

A. Future work

For certain parameters of the system, the nonlinearities might make it possible to obtain *spatially localized* normal modes where most of the energy is confined predominantly to one of the two beams⁴.

However, in my experimental setup, we were unable to achieve this due to the large degree of nonlinearities required. In the future, perhaps by using thinner beams and stronger magnets, we can observe this effect.

It would be interesting to investigate the critical parameter required to obtain such localized normal modes, especially because they are unique to nonlinear systems.

REFERENCES

- ¹D. Morin, *Introduction to classical mechanics with problems and solutions* (Cambridge University Press, 2019).
- ²M. Lakshmanan and S. Rajasekar, "Linear and nonlinear oscillators," in *Nonlinear Dynamics: Integrability, Chaos and Patterns* (Springer Berlin Heidelberg, Berlin, Heidelberg, 2003) pp. 17–30.
- ³International young Physicist's Tournament, "Problems for the 36th IYPT 2023," (2022).
- ⁴A. F. Vakakis, L. I. Manevitch, Y. V. Mikhlin, V. N. Pilipchuk, and A. A. Zevin, *Normal modes and localization in Nonlinear Systems* (Wiley, 1996).
- ⁵T. Irvine, "Bending frequencies of beams, rods, and pipes," (2012).
- ⁶N. F. Derby and S. Olbert, "Cylindrical magnets and ideal solenoids," *American Journal of Physics* **78**, 229–235 (2009).
- ⁷B. Fornberg, "Generation of finite difference formulas on arbitrarily spaced grids," *Mathematics of Computation* **51**, 699–706 (1988).
- ⁸J. C. Butcher, *Numerical methods for ordinary differential equations* (Wiley Online Library, 2008).
- ⁹D. Cline, "Introduction to Nonlinear Systems and Chaos," (2021), [Online; accessed 2024-01-01].
- ¹⁰V. C. Meesala, "Modeling and analysis of a cantilever beam tip mass system," (2018).

APPENDICES

Appendix A: Large deflection beam model derivation

Since the two beams are identical, we will focus on one beam in the derivation. The following derivation is based off the work of Meesala¹⁰ and the variables used are defined in Fig. 3.

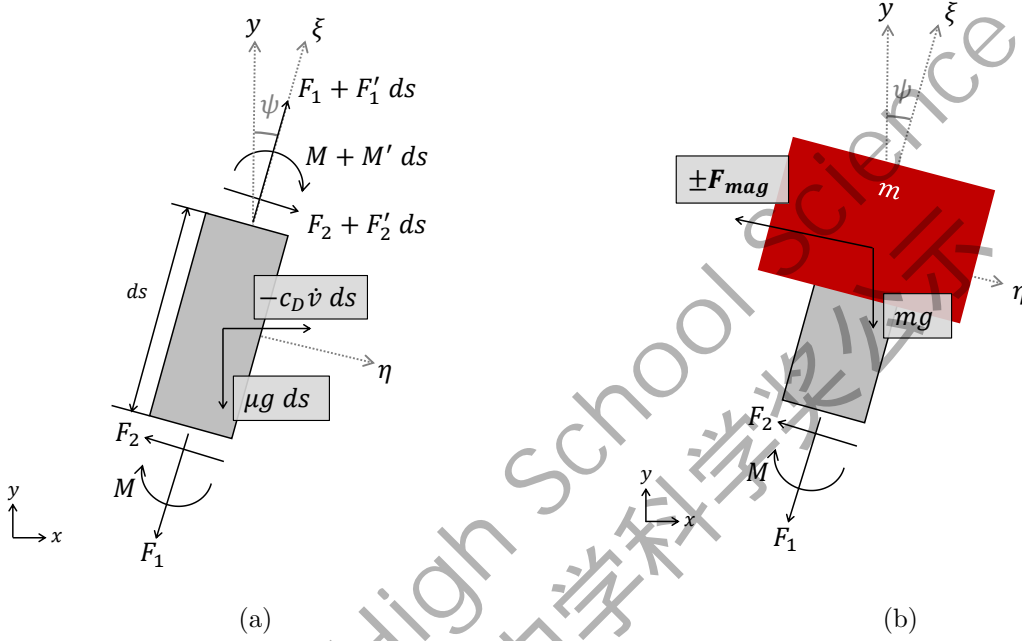


FIG. 9. I define a local orthogonal coordinate system ξ and η where ξ is along the axis of the beam and η is transverse to the beam axis. (a) Free body diagram for an infinitesimal beam segment of length ds . The internal forces acting on the beam element are the normal force F_1 , shear force F_2 , and the bending moment M . The external forces are its weight $\mu g ds$ and air drag $-c_D \dot{v} ds$. (b) Free body diagram for the tip of the beam. The forces are similar to that of the beam segment, along with the addition of the magnetic force \mathbf{F}_{mag} .

Zooming in on a small beam element of infinitesimal length ds (Fig. 9a), we define a local orthogonal coordinate system ξ and η as follows:

$$\begin{bmatrix} \hat{e}_\eta \\ \hat{e}_\xi \end{bmatrix} = \begin{bmatrix} \cos \psi & -\sin \psi \\ \sin \psi & \cos \psi \end{bmatrix} \begin{bmatrix} \hat{e}_x \\ \hat{e}_y \end{bmatrix}. \quad (\text{A1})$$

The internal forces acting on this beam are the normal force F_1 and the shear force F_2 , as well as the internal moment M about the z -axis. The external forces acting on the beam element are its weight $\mu g ds$ and air drag $-c_D \dot{v} ds$ where c_D is the damping

coefficient. With that, we can write down Newton's second law for this beam element:

$$\begin{aligned} & \left(\frac{\partial}{\partial s} (F_1 \hat{e}_\eta + F_2 \hat{e}_\xi) - \mu g \hat{e}_y - c_D \dot{v} \hat{e}_x \right) ds \\ & = \mu ds (\ddot{v} \hat{e}_x - \ddot{u} \hat{e}_y). \end{aligned} \quad (\text{A2})$$

In the RHS, I have subtracted $\ddot{u} \hat{e}_y$ in order to keep u positive.

We can do the same analysis for the tip of the beam (Fig. 9b), this time including the magnetic force:

$$\begin{aligned} \mathbf{F}_{\text{tip}} & = (-F_1 \hat{e}_\eta - F_2 \hat{e}_\xi)|_{s=L} - mg \hat{e}_y \pm \mathbf{F}_{\text{mag}} \\ & = m(\ddot{v} \hat{e}_x - \ddot{u} \hat{e}_y)|_{s=L}. \end{aligned} \quad (\text{A3})$$

Here, the $\pm \mathbf{F}_{\text{mag}}$ comes from the fact that depending on if we are looking at beam 1 or beam 2, the force can be positive or negative.

First, let us solve for the normal force F_1 . We can split Eqns. (A2) and (A3) into the x and y components:

Eq. (A2) x -component:

$$\frac{\partial}{\partial s} (F_1 \sin \psi + F_2 \cos \psi) - c_D \dot{v} = \mu \dot{v}, \quad (\text{A4})$$

Eq. (A2) y -component:

$$\frac{\partial}{\partial s} (F_1 \cos \psi - F_2 \sin \psi) - \mu g = -\mu \dot{u}, \quad (\text{A5})$$

Eq. (A3) x -component:

$$[-F_1 \sin \psi - F_2 \cos \psi - c_D \dot{v} \pm (\mathbf{F}_{\text{mag}} \cdot \hat{e}_\eta) \cos \psi \pm (\mathbf{F}_{\text{mag}} \cdot \hat{e}_\xi) \sin \psi]|_{s=L} = m \dot{v}|_{s=L}, \quad (\text{A6})$$

Eq. (A3) y -component:

$$[-F_1 \cos \psi + F_2 \sin \psi \mp (\mathbf{F}_{\text{mag}} \cdot \hat{e}_\eta) \sin \psi \pm (\mathbf{F}_{\text{mag}} \cdot \hat{e}_\xi) \cos \psi]|_{s=L} - mg = -m \dot{u}|_{s=L}. \quad (\text{A7})$$

We can integrate both sides of Eq. (A5) to obtain

$$\int_L^s \left[\frac{\partial}{\partial s} (F_1 \cos \psi - F_2 \sin \psi) - \mu g \right] ds = \int_L^s -\mu \dot{u} ds \quad (\text{A8})$$

$$\begin{aligned} & F_1 \cos \psi - F_2 \sin \psi - [F_1 \cos \psi - F_2 \sin \psi]|_{s=L} \\ & - \mu g (s - L) = -\mu \int_L^s \dot{u} ds. \end{aligned} \quad (\text{A9})$$

In order to obtain an expression for $[F_1 \cos \psi - F_2 \sin \psi]_{s=L}$ in Eq. (A9), we rearrange Eq. (A7):

$$\begin{aligned} [F_1 \cos \psi - F_2 \sin \psi]_{s=L} &= [m\ddot{u} \mp (\mathbf{F}_{\text{mag}} \cdot \hat{\mathbf{e}}_\eta) \sin \psi \\ &\quad \pm (\mathbf{F}_{\text{mag}} \cdot \hat{\mathbf{e}}_\xi) \cos \psi]_{s=L} - mg. \end{aligned} \quad (\text{A10})$$

We can then obtain an expression for F_1 by subbing Eq. (A10) into Eq. (A9) to obtain

$$\begin{aligned} F_1 &= \frac{1}{\cos \psi} \left\{ F_2 \sin \psi - mg + [(m\ddot{u} \mp (\mathbf{F}_{\text{mag}} \cdot \hat{\mathbf{e}}_\eta) \sin \psi \right. \\ &\quad \left. \pm (\mathbf{F}_{\text{mag}} \cdot \hat{\mathbf{e}}_\xi) \cos \psi)_{s=L}] \right. \\ &\quad \left. + \mu g(s - L) - \mu \int_L^s \ddot{u} ds \right\}. \end{aligned} \quad (\text{A11})$$

We solve for F_2 by balancing the moments about the z -axis:

$$M + F_2 ds = 0 \quad (\text{A12})$$

then applying moment-curvature relationship from Euler-Bernoulli beam theory:

$$M = EI\psi' \quad (\text{A13})$$

to obtain

$$F_2 = -EI\psi''. \quad (\text{A14})$$

In order to eliminate u from the equations, we apply the inextensibility constraint, meaning the beam's arc length has to remain constant. From Fig. 10, we arrive at the following two equations

$$\psi = \sin^{-1} v' \quad (\text{A15})$$

$$\cos \psi = \frac{ds - du}{ds} = 1 - u'. \quad (\text{A16})$$

After doing some Taylor expansions to 3rd order, we arrive at the relation

$$u' = \frac{1}{2}v'^2 + \mathcal{O}(v'^5). \quad (\text{A17})$$

Hence, u can be written in terms of v as

$$u(s, t) = \int_0^s u' dy = \int_0^s \frac{1}{2}v'^2 dy. \quad (\text{A18})$$

This equation will be used to eliminate u from the equations of motion.

We substitute in Eqs. (A11), (A14), (A18) back into Eq. (A4) and again do a Taylor expansion to third order, arriving at the following equation of motion for each cantilevered beam:

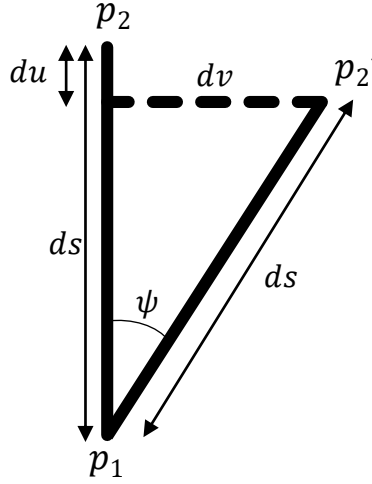


FIG. 10. The inextensibility constraint $p_1 p_2 = p_1 p_2'$ which states the beam has to remain the same length when it bends. Using this constraint, we can express u in terms of v (Eq. A18) to eliminate u from the equations.

$$\begin{aligned} \mu \ddot{v} + c_D \dot{v} + EI (v'''' + [v'(v'v'')]') + mgv'' + \frac{\mu}{2} \frac{\partial}{\partial s} \left(v' \int_L^s \int_0^\theta \frac{\partial^2}{\partial t^2} (v'^2) dy d\theta \right) \\ - \mu g (v' + (s-L)v'') - \frac{mv''}{2} \int_0^L \frac{\partial^2}{\partial t^2} (v'^2) ds \pm (\mathbf{F}_{\text{mag}} \cdot \hat{\mathbf{e}}_y) v'' = 0. \end{aligned} \quad (\text{A19})$$

Here, θ and y are dummy integration variables. This equation takes into account up to third order nonlinearities in the system.

One of the boundary conditions can be found by substituting Eqs. (A11), (A14), (A18) into Eq. (A6), once again expanding to third order:

$$\begin{aligned} m\ddot{v}|_{s=L} = & \left[mgv' - \frac{mv''}{2} \int_0^L \frac{\partial^2}{\partial t^2} (v'^2) dy \right. \\ & + EI (v'''' + v''''v'^2 + v''^2v') \\ & \pm (\mathbf{F}_{\text{mag}} \cdot \hat{\mathbf{e}}_x) \\ & \left. \pm (\mathbf{F}_{\text{mag}} \cdot \hat{\mathbf{e}}_y) \left(v' + \frac{1}{2}v'^3 \right) \right] \Big|_{s=L}. \end{aligned} \quad (\text{A20})$$

The remaining boundary conditions are moment equilibrium at the tip

$$v''(L, t) = 0, \quad (\text{A21})$$

and the geometric constraint at the fixed end that the displacement and angle must be

zero:

$$v(0, t) = v'(0, t) = 0 \quad (\text{A22})$$

Equations (A19) – (A22) are the full nonlinear equations describing the cantilevered beams.

Appendix B: Flexural rigidity characterisation

The flexural rigidity is the product of the Young's modulus E which is dependent on the beam material, and the second moment of area I which is dependent on the beam geometry. It appears in the moment-curvature relationship (Eq. A13) from Euler-Bernoulli beam theory. A higher value of EI means the beam is "stiffer" and bends less easily.

To measure this value for the beams used in my experiment, I clamped the beam to vibrate horizontally to eliminate the effects of gravity, then measured the frequency of small vibrations for different lengths. The data points were then fitted to the curve

$$\omega = \sqrt{\frac{3EI}{(0.2235\mu L + m)L^3}} \quad (\text{B1})$$

which came from Eq. (6) and (7) to find the value of EI (Fig. 11).

Appendix C: Method for determining beat and average frequency

Due to the effects of damping causing the amplitude as well as the frequency to decrease, taking the Fourier transform to find the modal frequencies does not give clear, sharp peaks, especially at larger amplitudes. Furthermore, due to practical limitations, I was only able to take data for a short time interval, causing the Fourier transform to be inaccurate and highly sensitive to the endpoint of the interval. As such, we are unable to accurately determine the two modal frequencies of the system from the Fourier transform. Here, we investigate the *initial* modal frequency of the system at the release amplitude. To address these issues, I investigated the initial beat and average frequency at the release amplitude. I found the peaks in the oscillation, then found the mean of the interval between each peak in just the first beat to find the average period, the reciprocal of which is the average frequency of just the first beat. The initial beat frequency is determined by fitting a curve in the form of $Ae^{-\beta t} |\sin((\omega_{\text{beat}} e^{-\gamma t}/2)t + \phi)|$ where I have

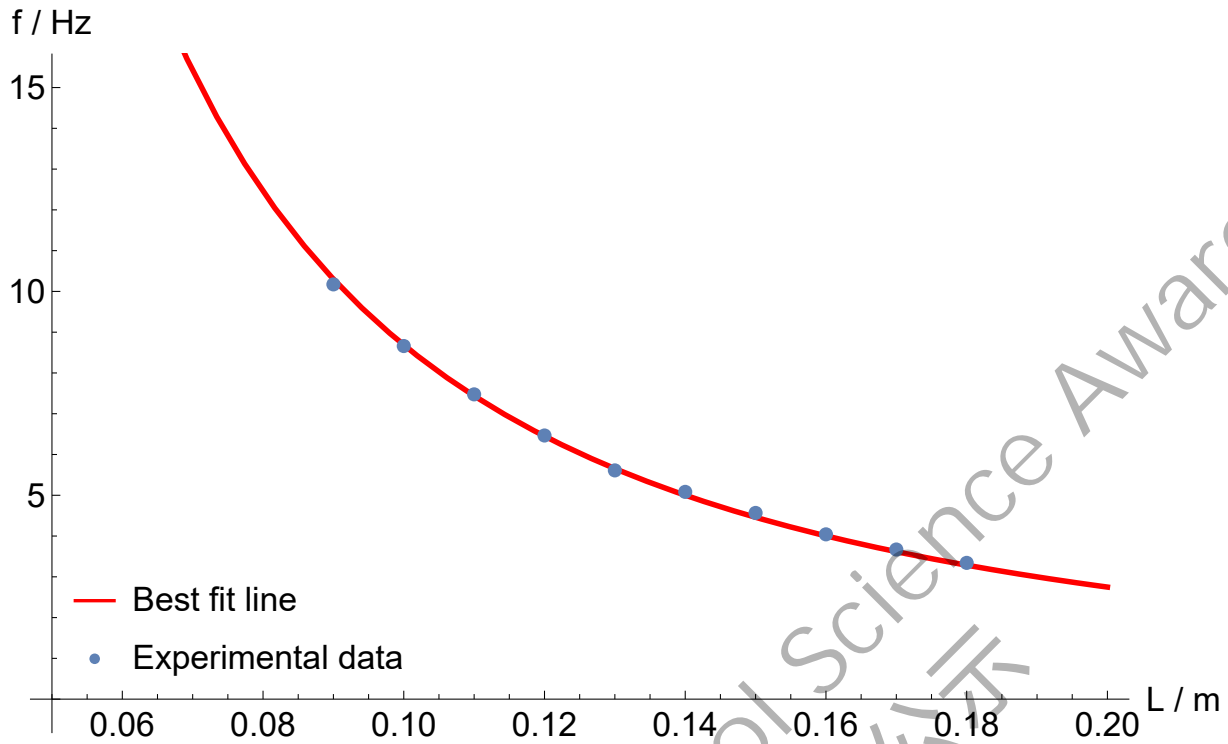


FIG. 11. Frequency-length plot used to measure the EI of the beams used, by find the best fit curve (red) to the data points (blue) using Eq. B1.

assumed the beat frequency decreases exponentially with time, following the amplitude which decreases exponentially with time due to linear damping (Fig. 12).

Appendix D: Effects of gravity

In order to investigate the effects of gravity, the MMO setup was tilted on its side to emulate the lack of gravity, and the setup was turned upside down to emulate gravity acting upwards.

	Average frequency / Hz	Beat frequency / Hz
Upright	6.42	0.425
Sideways	6.76	0.461
Upside-down	7.01	0.557

TABLE I. The beat and average frequencies of the MMO system when it is oriented upright, sideways, and upside-down to investigate the effects of gravity. We see a increasing trend in the frequencies as gravity goes from opposing the restoring spring force to being in the same direction as the restoring spring force.

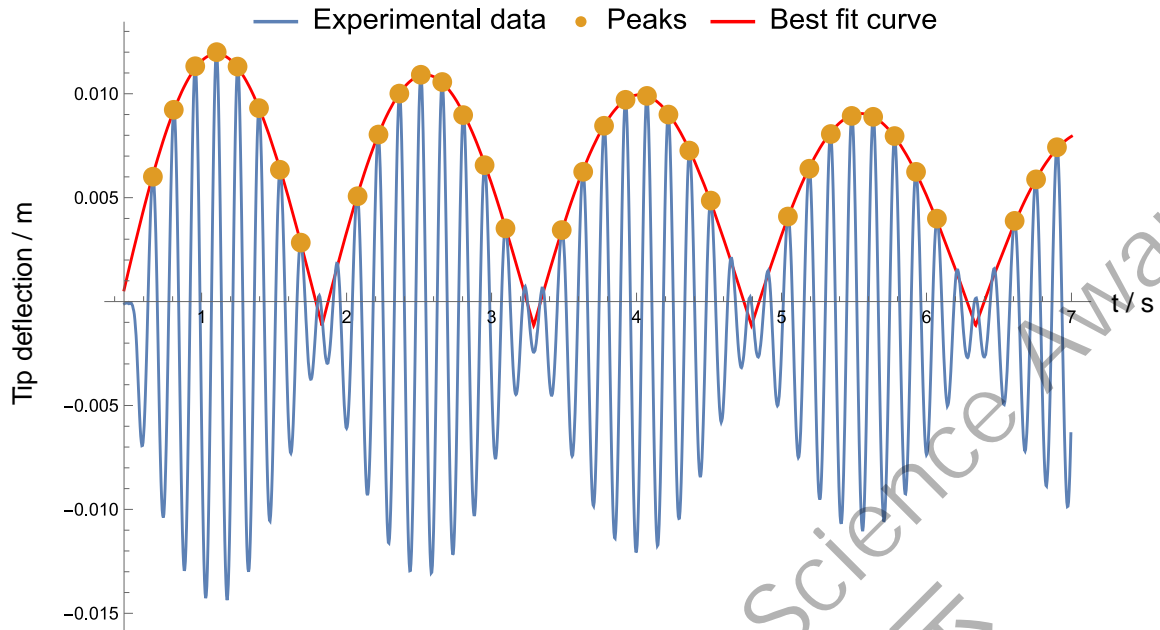


FIG. 12. The method used to determine the initial beat and average frequency. The peaks were found and the interval between the peaks in the first beat were used to determine the initial average frequency. The initial beat frequency was determined by fitting a sine curve with an exponentially decaying frequency to the peaks.

Experimentally, we see that the average and beat frequency increases as the setup is turned to sideways, then upside down (Table I). In the normal MMO setup, gravity is acting against the restoring force of the springs, while in the upside down case, gravity is acting in the same direction as the restoring force of the spring. The apparent spring constant of the leaf spring will increase as the setup is turned upside down, causing the increase in the average and beat frequency.

Appendix E: Orders of magnitude of nonlinear terms

Term	Order of magnitude / N m^{-1}
Damping $c_D \dot{v}$	10^{-2}
Spring force $EI v''''$	1
Nonlinear spring force $EI [v'(v'v'')]'$	10^{-1}
Nonlinear curvature $\frac{\mu}{2} \frac{\partial}{\partial s} \left(v' \int_L^s \int_0^\theta \frac{\partial^2}{\partial t^2} (v'^2) dy d\theta \right)$	10^{-1}
Tip mass mgv''	10^{-1}
Gravity $\mu g(v' + (s - L)v'')$	10^{-1}
Nonlinear curvature (tip mass) $\frac{mv''}{2} \int_0^L \frac{\partial^2}{\partial t^2} (v'^2) ds$	10^{-1}
Magnetic force term $(\mathbf{F}_{\text{mag}} \cdot \hat{\mathbf{e}}_y)v''$	10^{-6}

TABLE II. Maximum orders of magnitude of different terms in Eq. (27), for a initial displacement of 1 cm, length $L = 12$ cm, and separation distance $d_0 = 5$ cm.

Term	Order of magnitude / N
Spring force EIv'''	10^{-1}
Nonlinear spring force $EI(v''v'^2 + v''^2v')$	10^{-3}
Tip mass mgv'	10^{-2}
Nonlinear tip mass $\frac{mv''}{2} \int_0^L \frac{\partial^2}{\partial t^2}(v'^2) dy$	10^{-3}
x-component magnetic force $(\mathbf{F}_{\text{mag}} \cdot \hat{\mathbf{e}}_x)$	10^{-2}
y-component magnetic force $(\mathbf{F}_{\text{mag}} \cdot \hat{\mathbf{e}}_y)$	10^{-3}
Magnetic force term $(\mathbf{F}_{\text{mag}} \cdot \hat{\mathbf{e}}_y)(v' + \frac{1}{2}v'^3)$	10^{-4}

TABLE III. Maximum orders of magnitude of different terms in Eq. (28), for a initial displacement of 1 cm, length $L = 12$ cm, and separation distance $d_0 = 5$ cm.